Int. J. Solids Structures Vol. 14, pp. 591–610

0020-7683/78/0701-0591/$02.00/0

INELASTIC STABILITY OF DIAGONAL BRACES IN BUILDING FRAMES†

SHOSUKE MORINO
Department of Architecture, Kyushu University, Fukuoka, Japan

SUPACHAI LIMPISVASTI
Technical Division, The Royal Thai Air Force, Bangkok, Thailand

and

SENG-LIP LEE
Department of Civil Engineering, University of Singapore, Singapore

(*Received* 21 *March* 1977; *in revised form* 27 *January* 1978; *received for publication* 15 *February* 1978)

Abstract—The inelastic behavior of diagonal braces in building frames subjected to relative horizontal end displacements is investigated both theoretically and experimentally with particular reference to the post-buckling behavior. The analysis is based on commonly adopted piecewise linear approximate moment-thrust interaction curves and bilinear elastic–plastic moment-curvature relations. The maximum loads as well as the horizontal load-displacement curves observed in the experimental investigation agree well with the theoretical prediction for short braces. In the medium range, the stable branches of the horizontal load-displacement curves are followed by a steep unloading branch, with initially positive slope which becomes infinite at a point beyond which the curves become unstable. The maximum experimental loads are smaller than the theoretical predictions and occur consistently in the vicinity of the point of infinite slope in the theoretical horizontal load-displacement curves. The experimental curves start to deviate from the theoretical curves shortly before reaching this point, showing rapid increase in the displacement. Finally, long braces behave elastically until the maximum loads are attained at the termination of the elastic state. For practical purposes, a simple means for predicting the carrying capacity of diagonal braces is recommended in view of these findings.

NOTATION

A cross-sectional area
$B_1, \ldots, B_6$ functions of ϕ defined in eqns (29c) and (31a–e)
d depth of the wide-flange section
E modulus of elasticity
E_t tangent modulus
f shape factor
H horizontal load
h H/P_y, non-dimensional horizontal load
I moment of inertia
l length of the brace
M bending moment
M_p full plastic bending moment
m M/M_p, non-dimensional bending moment
P axial force
P_y yield axial force
p P/P_y, non-dimensional axial force
R ratio of the flange area to the web area
r radius of gyration
V shear force
v V/P_y, non-dimensional shear force
x, y coordinate system
Z_p plastic section modulus
α non-dimensional plastic hinge rotation
Δ horizontal displacement
δ $\Delta/(l\sqrt{\epsilon_y})$, non-dimensional horizontal displacement
ϵ_y yield strain
η $y/(l\sqrt{\epsilon_y})$, non-dimensional lateral deflection
θ inclination angle of the brace
λ $\sqrt{\epsilon_y}(l/r)$, normalized slenderness ratio
μ $l/(Z_p r)$
ξ x/l
$\sigma_c, \sigma_p, \sigma_y$ critical stress, proportional limit stress and yield stress, respectively
τ E_t/E, tangent modulus ratio
ϕ $l\sqrt{[P/(EI)]}$

†The research upon which this paper is based was done when the authors were associated with the Division of Structural Engineering and Mechanics, Asian Institute of Technology, Bangkok, Thailand.

1. INTRODUCTION

Diagonal bracing systems are recently used for preventing excessive lateral displacement and improving the lateral stiffness of high-rise structures. The inelastic stability of diagonal braces subjected to relative horizontal end displacements is of practical importance in the design of such structural systems.

The behavior of simply supported and axially loaded compression members, including the post-buckling range, was investigated by Paris[1], in which he assumed that the column takes a sinusoidal deformed shape and the post-buckling range is characterized by the formation of a plastic hinge at the mid-height after the axial load reaches either the yield load or the Euler load depending upon the slenderness ratio. Murray[2, 3] and Nutt[4] investigated the behavior of the compression members in triangular frames, assuming that the compression member is eccentrically loaded and deflection increases hyperbolically as the load increases and approaches the critical load in the elastic range. The elastic limit is obtained by considering, for the post-buckling range, a mechanism formed by the development of plastic hinges in the member. Neal and Griffith[5] investigated the behavior and collapse loads of rigidly jointed redundant trusses both theoretically and experimentally, using axial load-deformation relations obtained from tests.

Wakabayashi *et al.*[6] predicted the hysteretic behavior of braced frames, in which the analysis of a simply supported brace subjected to repeated tension-compression loading was carried out by extending the work done by Paris[1].

Igarashi *et al.*[7] derived a solution of the hysteretic behavior of a simply supported bar under repeated loading by an incremental analysis based on the non-linear yield condition for a rectangular cross section. Nonaka[8] approached the same problem, considering the plastic interaction for the combined action of bending and axial deformation based on a piecewise linear yield condition. Similar work was done by Higginbotham[9], who considered the curvature-deflection relation based on finite deflection theory, and obtained the solution of the same problem in terms of elliptic integrals. Shibata *et al.*[10] assumed that the bending deformation concentrates in the middle portion of the bar, the remaining portion having infinite rigidity in bending, and Wada, Suto and Fujimoto[11] analysed *K*-type braced frames by dividing the member into small elements to take into account the effect of the yield zone spreading along the longitudinal axis and the strain reversal in the cross section.

In all the theoretical works mentioned above, the brace is treated as a bar subjected to axial load only, assuming that both ends of the bar are simply supported. In current high-rise building construction, the diagonal braces are often rigidly connected to the beam-column system. When such a braced frame is subjected to horizontal loads, relative horizontal story displacement causes both bending moment and axial thrust (Fig. 1). The purpose of the present study is to analyse the elastic–plastic behavior of such a brace with particular reference to the determination of the load carrying capacity and the post-buckling behavior. The results of experi-

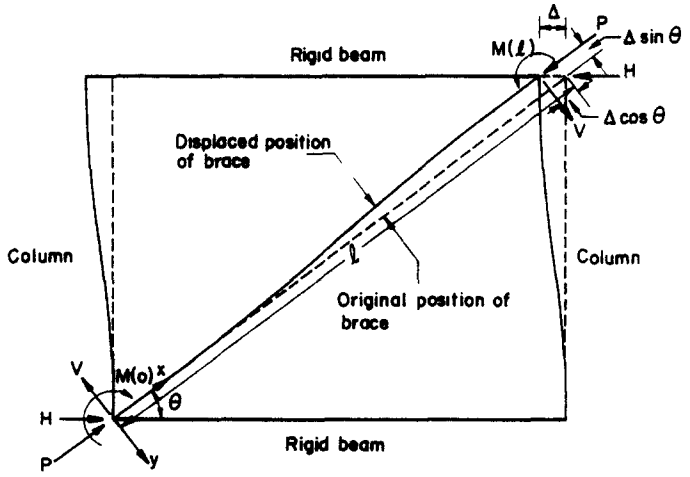

Fig. 1. Model of a diagonal brace in building frames.

mental investigations are compared with predicted values obtained from the theoretical analysis, and simple charts and equations for the determination of the load carrying capacity are presented to facilitate the design of such braces.

2. THEORETICAL INVESTIGATION

Fundamental consideration

The model proposed in this study is an initially straight, inclined bar of length l, restrained against rotation at both ends and subjected to a horizontal displacement at the top end while the bottom end remains at the original position, as shown in Fig. 1. The coordinate system is taken such that the poxitive x-axis is along the longitudinal axis of the brace with the origin at the bottom end and the positive y-axis is downward. The inclination angle θ is measured between the brace and the beam. The stress resultants are positive as shown, $M(l)$ and $M(0)$ being the end moments at the top and bottom ends, respectively, and V the shear force. The axial force P is positive in compression. The horizontal load H and the horizontal displacement Δ are shown in Fig. 1 in the positive directions.

The following assumptions are made to simplify the problem. The top and botton beams to which the brace is rigidly connected are infinitely rigid compared to the brace, and only horizontal relative rigid body displacement is allowed under the action of the horizontal load H. The brace is prismatic and made of wide-flange or box section, the moment-curvature relation is elastic–plastic, deflections are small, the effect of residual stress is not considered, and only plane buckling in the plane of the web is allowed. The yield condition adopted is as follows:

$$|m| = 1 \qquad \text{for} \quad p \leq 0.15 \tag{1}$$

$$|m| = 1.18(1-p) \quad \text{for} \quad p > 0.15 \tag{2}$$

in which $m = M/M_p$ and $p = P/P_y$; M_p and P_y denoting the plastic bending moment and the yield axial force respectively. In Fig. 2, actual and approximate interaction curves for wide-flange sections are shown together with those for a box section which will be used in the experimental investigation.

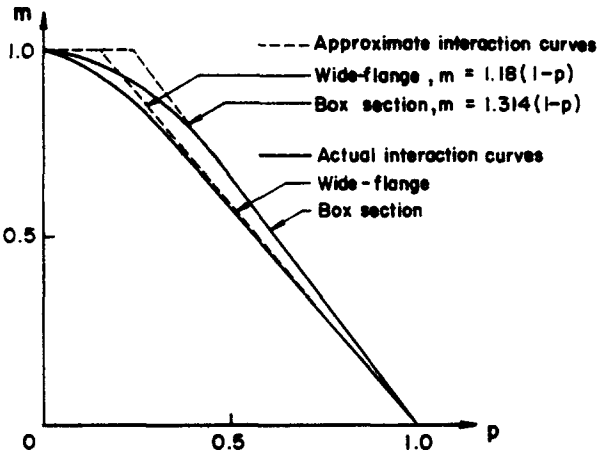

Fig. 2. Actual and approximate interaction curves.

Elastic state

The deformation of an axially loaded prismatic column subjected to end forces is governed by

$$\frac{d^4\eta}{d\xi^4} + \phi^2 \frac{d^2\eta}{d\xi^2} = 0 \tag{3}$$

in which $\eta = y/(l\sqrt{\epsilon_y})$, $\xi = x/l$, $\phi = \sqrt{[Pl^2/(EI)]}$ and E, I and ϵ_y denote the modulus of elasticity, the moment of inertia and the yield strain of the material, respectively. Referring to

Fig. 1, the boundary conditions for the elastic state are as follows:

$$\text{at} \quad \xi = 0, \quad \eta = \frac{d\eta}{d\xi} = 0 \tag{4a}$$

$$\text{at} \quad \xi = 1, \quad \eta = -\delta \sin\theta; \quad \frac{d\eta}{d\xi} = 0 \tag{4b}$$

where $\delta = \Delta/(l\sqrt{\epsilon_y})$. The solution of eqn (3) subject to eqns (5a, b) takes the form

$$\eta(\xi) = \delta \sin\theta \frac{\sin\phi\left(\frac{1}{2}-\xi\right) - \sin\frac{\phi}{2} + \phi\xi\cos\frac{\phi}{2}}{2\left(\sin\frac{\phi}{2} - \frac{\phi}{2}\cos\frac{\phi}{2}\right)}. \tag{5}$$

The total shortening of the brace is equal to the shortening caused by the axial force in addition to the shortening due to the deflected configuration, i.e.

$$\frac{\delta}{\sqrt{\epsilon_y}}\cos\theta = \left(\frac{\phi}{\lambda}\right)^2 + \frac{1}{2}\int_0^1 \left(\frac{d\eta}{d\xi}\right)^2 d\xi \tag{6}$$

in which $\lambda = \sqrt{\epsilon_y}(l/r)$ the normalized slenderness ratio of the brace, $r = \sqrt{(I/A)}$, and A denotes the cross-sectional area. Substituting eqn (5) into eqn (6) leads to

$$\frac{\delta}{\sqrt{\epsilon_y}}\cos\theta = \left(\frac{\phi}{\lambda}\right)^2 + \delta^2\sin^2\theta \frac{\phi\{\phi(2+\cos\phi) - 3\sin\phi\}}{16\left(\sin\frac{\phi}{2} - \frac{\phi}{2}\cos\frac{\phi}{2}\right)^2} \tag{7}$$

which is the equation governing the elastic behavior of the brace, relating δ to ϕ and λ. Observe in the governing equation that ϵ_y remains a parameter in the term due to the axial constraint in the boundary conditions.

In view of eqn (5), the non-dimensional moment m and horizontal load $h = H/P_y$, where H denotes the horizontal load, can be expressed by

$$m(\xi) = -\left(\frac{\mu}{\lambda}\right)\frac{d^2\eta}{d\xi^2} = \left(\frac{\mu}{\lambda}\right)\delta\sin\theta \frac{\phi^2\sin\phi\,(1/2-\xi)}{2\left(\sin\frac{\phi}{2} - \frac{\phi}{2}\cos\frac{\phi}{2}\right)} \tag{8}$$

$$h = p\cos\theta - v\sin\theta = \left(\frac{\phi}{2}\right)^2\left\{\cos\theta + \delta\sqrt{\epsilon_y}\sin^2\theta \frac{\frac{\phi}{2}\cos\frac{\phi}{2}}{\sin\frac{\phi}{2} - \frac{\phi}{2}\cos\frac{\phi}{2}}\right. \tag{9}$$

where $\mu = I/Z_p r$, $v = V/P_y$, Z_p denotes the plastic section modulus of the brace and V the shear force. Note that $p = (\phi/\lambda)^2$.

The elastic state is terminated when the yield condition is satisfied at any point along the brace. Since the axial force P is predominant, i.e. $p > 0.15$, eqn (2) is the yield condition under consideration and is rewritten for convenience in the form

$$|m| = 1.81\left\{1 - \left(\frac{\phi}{\lambda}\right)^2\right\}. \tag{10}$$

The first plastic hinge forms at the point along the brace where

$$\frac{dm}{d\xi} = 0 \tag{11}$$

or at the boundary. It should be noted that eqn (8) shows the antisymmetrical nature of the bending moment distribution, i.e. $m(\xi) = -m(1-\xi)$. Supposing that $\xi = \xi^*$ satisfies eqn (11), the maximum absolute value of the bending moment occurs at $\xi = \xi^*$ and $\xi = 1-\xi^*$, simultaneously, if $0 < \xi^* < 1$. On the other hand if $\xi^* \leq 0$ or $1 \leq \xi^*$, the first pair of plastic hinges appear at both ends of the brace. Substituting eqn (8) into eqn (11) gives the relation between ξ^* and ϕ under the condition $\xi^* < 1/2$ as

$$\xi^* = \frac{\phi - \pi}{2\phi}. \tag{12}$$

It is obvious that if $0 \leq \phi \leq \pi$, $\xi^* \leq 0$, i.e. the maximum absolute value of the bending moment occurs at the ends of the brace and that, if $\phi > \pi$, the maximum absolute value of the bending moment occurs at the interior points, $\xi = \xi^*$ and $\xi = 1-\xi^*$.

Let λ^* be the normalized slenderness ratio at which the first pair of plastic hinges form at both ends when $\phi = \pi$. The bending moments at the ends $m(0)$ and $m(1)$, must satisfy eqn (10) together with the axial force parameter $\phi = \pi$. Substituting $\phi = \pi$ and $\lambda = \lambda^*$ in eqns (10) and (7), in view of eqn (8), leads to two equations relating δ to λ^*.

Eliminating δ from these two equations yields the value of λ^*, the limiting value of the normalized slenderness ratio between the ranges $\lambda < \lambda^*$, in which the first pair of plastic hinges form at both ends, and $\lambda \geq \lambda^*$, in which the first pair of plastic hinges form at the interior points. The values of λ^* for various values of θ and ϵ_y are tabulated in Table 1, assuming that $\mu = 1.05$, which is approximately the average value for all wide-flange column sections as will be explained later. The bending moments $m(0)$ and $m(\xi^*)$ are determined by eqns (8) and (12). An examination of the expression $m(\xi^*)$ shows that, for positive values of δ, $m(\xi^*)$ is always positive as long as $\phi < 8.986$, $\phi = 8.986$ being the smallest root of equation obtained by setting the denominator in eqn (8) equal to zero.

Table 1. Values of λ^* and $\hat{\lambda}$ for $\mu = 1.05$

ϵ_y	θ	λ^*	$\hat{\lambda}$
0.0012	30°	3.18	6.45
	45°	3.21	6.56
	60°	3.27	6.76
0.0013	30°	3.18	6.46
	45°	3.22	6.58
	60°	3.27	6.78
0.0014	30°	3.18	6.47
	45°	3.22	6.59
	60°	3.27	6.81
0.0015	30°	3.19	6.48
	45°	3.22	6.59
	60°	3.28	6.82

For $\lambda < \lambda^*$, substituting $m(0)$ into eqn (10) leads to

$$\left(\frac{\mu}{\lambda}\right)\delta \sin\theta \frac{\phi^2 \sin\frac{\phi}{2}}{2\left(\sin\frac{\phi}{2} - \frac{\phi}{2}\cos\frac{\phi}{2}\right)} = 1.18\left\{1 - \left(\frac{\phi}{\lambda}\right)^2\right\} \quad \text{for} \quad 0 < \lambda < \lambda^*. \tag{13}$$

Note that $m(0)$ is positive in the range $0 < \phi < 2\pi$, which is always satisfied in this case. On the other hand, for $\lambda \geq \lambda^*$, substituting $m(\xi^*)$ into eqn (10) leads to

$$\left(\frac{\mu}{\lambda}\right)\delta \sin\theta \frac{\phi^2}{2\left(\sin\frac{\phi}{2} - \frac{\phi}{2}\cos\frac{\phi}{2}\right)} = 1.18\left\{1 - \left(\frac{\phi}{\lambda}\right)^2\right\} \quad \text{for} \quad \lambda \geq \lambda^*. \tag{14}$$

Elastic–plastic state

The elastic state is terminated when, for a given value of λ, δ and ϕ satisfy eqn (7) and either eqns (13) or (14).

Case 1: $0<\lambda<\lambda^*$. In this case, plastic hinges form at both ends of the brace and the constants of integration in the solution of eqn (3) are determined, in view of eqn (10), from the following boundary conditions:

$$\text{at} \quad \xi=0, \quad \eta=0; \qquad m(0)=1.18(1-p) \tag{15a}$$

$$\text{at} \quad \xi=1, \quad \eta=-\delta\sin\theta; \quad -m(1)=1.18(1-p) \tag{15b}$$

and the deflection is obtained in the form

$$\eta(\xi)=1.18\left(\frac{\lambda}{\mu\phi^2}\right)\left\{1-\left(\frac{\phi}{\lambda}\right)^2\right\}\left\{\frac{\sin\phi(1-\xi)-\sin\phi\xi}{\sin\phi}+2\xi-1\right\}-\delta\xi\sin\theta. \tag{16}$$

Substituting eqn (16) into eqn (6) leads to

$$\frac{\delta}{\sqrt{\epsilon_y}}\cos\theta=\left(\frac{\phi}{\lambda}\right)^2+\frac{1}{2}\delta^2\sin^2\theta+\left(1.18\frac{\lambda}{\mu}\right)^2\left\{1-\left(\frac{\phi}{\lambda}\right)^2\right\}\frac{\phi(1+\cos\phi)(\phi+\sin\phi)-4\sin^2\phi}{2\phi^4\sin^2\phi} \tag{17}$$

and the bending moment is obtained as

$$m(\xi)=1.18\left\{1-\left(\frac{\phi}{\lambda}\right)^2\right\}\frac{\sin\phi(1-\xi)-\sin\phi\xi}{\sin\phi}. \tag{18}$$

The horizontal force becomes, in this case,

$$h=\left(\frac{\varphi}{\lambda}\right)^2\left[\cos\theta+2.36\sin\theta\left(\frac{\lambda\sqrt{\epsilon_y}}{\mu\varphi^2}\right)\left\{1-\left(\frac{\varphi}{\lambda}\right)^2\right\}-\delta\sqrt{\epsilon_y}\sin^2\theta\right]. \tag{19}$$

Case 1(a): $0<\lambda\leq\bar{\lambda}$. Equation (16) remains valid as long as $\varphi\leq\pi$ when plastic collapse occurs by axial yielding, i.e. when $p=1$. The upper limit of λ in this case, $\bar{\lambda}$, is obtained by setting $\varphi=\pi$ when $P=P_y$, i.e.

$$\varphi=l\sqrt{\left(\frac{P_y}{EI}\right)}=\bar{\lambda}=\pi. \tag{20}$$

The values of λ^* in Table 1 show that $\bar{\lambda}<\lambda^*$, and that the range $\bar{\lambda}<\lambda<\lambda^*$ is relatively narrow.

The behavior of a brace in the range, $0<\lambda\leq\bar{\lambda}$, is shown in Fig. 3, in which the numbers 1–4 denote, respectively, a typical elastic state, the termination of the elastic state, a typical elastic–plastic state and incipient plastic collapse state by axial yielding. In Fig. 3(c), the stress points for all values of ξ lie on a vertical line at every stage of loading as p is constant with respect to ξ, and the path for $\xi=0.5$ lies on the p-axis as $m=0$ at this point due to anti-symmetry. In accordance with previous discussion, Fig. 3(d) clearly shows that the moment is maximum at $\xi=0$ for all stages of loading.

Case 1(b): $\bar{\lambda}<\lambda<\lambda^*$. In this range of λ, eqn (16) remains valid until $\varphi=\pi$ when the plastic hinges at the ends unload and the brace behaves elastically for $\varphi>\pi$ with the following boundary conditions:

$$\text{at} \quad \xi=0, \quad \eta=0; \qquad \frac{d\eta}{d\xi}=\alpha \tag{21a}$$

$$\text{at} \quad \xi=1, \quad \eta=-\delta\sin\theta; \quad \frac{d\eta}{d\xi}=\alpha \tag{21b}$$

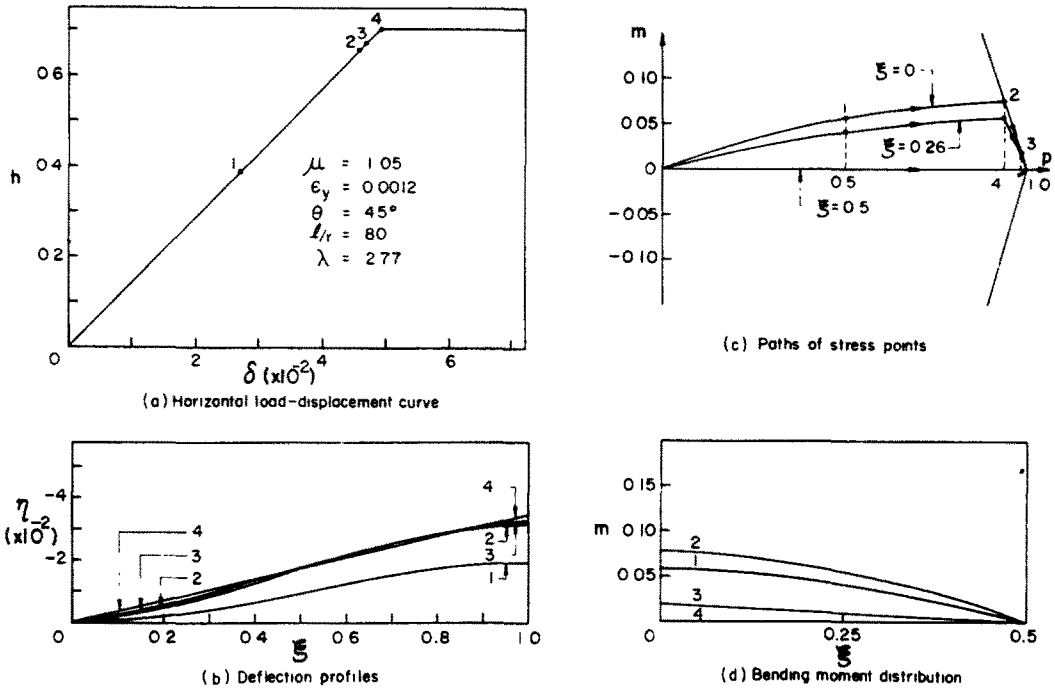

Fig. 3. Behavior of a short brace, Case 1(a).

in which α is negative and calculated from eqn (16) at $\varphi = \pi$. The solution of eqn (3) in this case takes the form

$$\eta(\xi) = (\alpha + \delta \sin\theta)\frac{\sin\varphi\left(\frac{1}{2}-\xi\right) - \sin\frac{\varphi}{2} + \varphi\xi\cos\frac{\varphi}{2}}{2\left(\sin\frac{\varphi}{2} - \frac{\varphi}{2}\cos\frac{\varphi}{2}\right)} + \alpha\xi. \tag{22}$$

Substituting eqn (22) into eqn (6) leads to

$$\frac{\delta}{\sqrt{\epsilon_y}}\cos\theta = \left(\frac{\phi}{\lambda}\right)^2 + (\alpha + \delta\sin\theta)^2\frac{\phi\{\phi(2+\cos\phi) - 3\sin\phi\}}{16\left(\sin\frac{\phi}{2} - \frac{\phi}{2}\cos\frac{\phi}{2}\right)^2} - \alpha\left(\frac{\alpha}{2} + \delta\sin\theta\right) \tag{23}$$

and the bending moment becomes

$$m(\xi) = \left(\frac{\mu}{\lambda}\right)(\alpha + \delta\sin\theta)\frac{\phi^2\sin\phi\left(\frac{1}{2}-\xi\right)}{2\left(\sin\frac{\phi}{2} - \frac{\phi}{2}\cos\frac{\phi}{2}\right)}. \tag{24}$$

The horizontal force in this case becomes

$$h = \left(\frac{\phi}{\lambda}\right)^2\left[\cos\theta + \sqrt{\epsilon_y}\sin\theta\frac{\delta\sin\theta\left(\phi\cos\frac{\phi}{2}\right) + 2\alpha\sin\frac{\phi}{2}}{2\left(\sin\frac{\phi}{2} - \frac{\phi}{2}\cos\frac{\phi}{2}\right)}\right]. \tag{25}$$

This elastic state terminates when plastic hinges form at $\xi = \bar{\xi}$ and $\xi = 1 - \bar{\xi}$ such that $\bar{\xi}$ satisfies eqn (11). Substituting eqn (24) in eqn (11) yields, for $\bar{\xi} < 1/2$,

$$\bar{\xi} = \frac{\phi - \pi}{2\phi}. \tag{26}$$

Substituting eqn (24) with $\xi = \bar{\xi}$ in eqn (10) leads to

$$\left(\frac{\mu}{\lambda}\right)(\alpha + \delta \sin\theta)\frac{\phi^2}{2\left(\sin\frac{\phi}{2} - \frac{\phi}{2}\cos\frac{\phi}{2}\right)} = 1.18\left\{1 - \left(\frac{\phi}{\lambda}\right)^2\right\} \quad \text{for} \quad \bar{\lambda} < \lambda < \lambda^* \tag{27}$$

The solution of eqns (23) and (27) for ϕ and δ determines the termination of the elastic state in this case.

For further loading, the plastic hinges at $\xi = \bar{\xi}$ and $\xi = 1 - \bar{\xi}$ divide the brace into three domains. Taking advantage of anti-symmetry, only two domains, i.e. $0 \leq \xi \leq \bar{\xi}$ and $\bar{\xi} \leq \xi \leq 1/2$, need be considered with the respective solutions, $\eta_1(\xi)$ and $\eta_2(\xi)$, which contains 8 constants of integration. The boundary and continuity conditions are:

$$\text{at} \quad \xi = 0; \quad \eta_1 = 0; \quad \frac{d\eta_1}{d\xi} = \alpha \tag{28a}$$

$$\text{at} \quad \xi = \bar{\xi}; \quad \eta_1 = \eta_2; \quad m_1(\bar{\xi}) = m_2(\bar{\xi}) = 1.18(1-p); \quad v_1(\bar{\xi}) = v_2(\bar{\xi}) \tag{28b}$$

$$\text{at} \quad \xi = 1/2; \quad \eta_2 = -\frac{\delta}{2}\sin\theta; \quad m_2\left(\frac{1}{2}\right) = 0. \tag{28c}$$

In view of eqns (28a–c), the solutions take the form

$$\eta_1(\xi) = \frac{1}{B_1}\left[\frac{1.18\lambda}{\mu\varphi^2}\left\{1 - \left(\frac{\varphi}{\lambda}\right)^2\right\}\{2\sin\varphi\xi - \varphi\cos\varphi\xi + \varphi(1-2\xi)\} - \delta\sin\theta\{\sin\varphi(\xi - \bar{\xi}) - \varphi\xi\cos\varphi\bar{\xi} + \sin\varphi\bar{\xi}\} - \alpha\{\sin\varphi(\xi - \bar{\xi}) + (1-2\xi)\sin\varphi\bar{\xi}\}\right] \quad \text{for} \quad 0 \leq \xi \leq \bar{\xi} \tag{29a}$$

$$\eta_2(\xi) = \frac{1}{B_1}\left[\frac{1.18\lambda}{\mu\varphi^2}\left\{1 - \left(\frac{\varphi}{\lambda}\right)^2\right\}\left\{B_1\frac{\sin\varphi(1/2 - \xi)}{\sin\varphi(1/2 - \bar{\xi})} + \varphi(1-2\xi)\right\} - \delta\sin\theta(\sin\varphi\bar{\xi} - \varphi\xi\cos\varphi\bar{\xi}) - \alpha(1-2\xi)\sin\varphi\bar{\xi}\right] \quad \text{for} \quad \bar{\xi} \leq \xi \leq \frac{1}{2} \tag{29b}$$

in which

$$B_1 = 2\sin\varphi\bar{\xi} - \varphi\cos\varphi\bar{\xi}. \tag{29c}$$

Substituting eqns (29a–c) in eqn (6) leads to

$$\frac{\delta^\bullet}{\sqrt{\epsilon_y}}\cos\theta = \left(\frac{\varphi}{\lambda}\right)^2 + \frac{\varphi^2\bar{\xi}}{2}(B_3^2 + B_4^2 - B_5^2 - B_6^2) + \frac{\varphi}{4}(B_3^2 - B_4^2 - B_5^2 + B_6^2)\sin 2\varphi\bar{\xi} + \frac{\varphi^2}{4}(B_5^2 + B_6^2) + \frac{\varphi}{4}(B_5^2 - B_6^2)\sin\varphi + \frac{\varphi}{2}\{(B_3B_4 - B_5B_6)\cos 2\varphi\bar{\xi} - B_3B_4 - B_5B_6\cos\varphi\} + 2B_2\left\{\frac{B_2}{4} + B_3\sin\varphi\bar{\xi} + B_4(\cos\varphi\bar{\xi} - 1) + B_5(\sin\varphi - \sin 2\varphi\bar{\xi}) + B_6\left(\cos\frac{\varphi}{2} - \cos\varphi\bar{\xi}\right)\right\} \tag{30}$$

in which

$$B_2 = -\frac{1}{B_1}\left[\frac{2.36\lambda}{\mu\varphi}\left\{1 - \left(\frac{\varphi}{\lambda}\right)^2\right\} - \delta\sin\theta(\varphi\cos\varphi\bar{\xi}) - 2\alpha\sin\varphi\bar{\xi}\right] \tag{31a}$$

$$B_3 = \frac{\alpha - B_2}{\varphi} \tag{31b}$$

$$B_4 = -\frac{1}{B_1}\left[\frac{1.18\lambda}{\mu\varphi}\left\{1-\left(\frac{\varphi}{\lambda}\right)^2\right\} - (\alpha + \delta \sin\theta)\sin\varphi\bar{\xi}\right] \tag{31c}$$

$$B_5 = -\left(\frac{1.18\lambda}{\mu\varphi^2}\right)\left\{1-\left(\frac{\varphi}{\lambda}\right)^2\right\}\frac{\cos\varphi/2}{\sin\varphi(1/2-\bar{\xi})} \tag{31d}$$

$$B_6 = -B_5 \tan\frac{\varphi}{2}. \tag{31e}$$

In view of eqns (29a–c), the bending moments and horizontal force are obtained as

$$m_1(\xi) = \frac{1}{B_1}\left[1.18\left\{1-\left(\frac{\varphi}{\lambda}\right)^2\right\}(2\sin\varphi\xi - \varphi\cos\varphi\xi) - \frac{\mu\varphi^2}{\lambda}(\alpha + \delta\sin\theta)\sin\varphi(\xi-\bar{\xi})\right] \tag{32a}$$

$$m_2(\xi) = 1.18\left\{1-\left(\frac{\varphi}{\lambda}\right)^2\right\}\frac{\sin\varphi(1/2-\xi)}{\sin\varphi(1/2-\bar{\xi})} \tag{32b}$$

$$h = \left(\frac{\varphi}{\lambda}\right)^2\left[\cos\theta - \frac{\sqrt{\epsilon_y}\sin\theta}{B_1}\left\{\frac{2.36\lambda}{\mu\varphi}\left\{1-\left(\frac{\varphi}{\lambda}\right)^2\right\} - \delta\sin\theta\,(\varphi\cos\varphi\bar{\xi}) - 2\alpha\sin\varphi\bar{\xi}\right\}\right]. \tag{33}$$

Substituting eqn (32a) in eqn (10) with $\xi = 0$ leads to

$$\frac{1}{B_1}\left[-1.18\varphi\left\{1-\left(\frac{\varphi}{\lambda}\right)^2\right\} + \frac{\mu\varphi^2}{\lambda}(\alpha+\delta\sin\theta)\sin\varphi\bar{\xi}\right] = 1.18\left\{1-\left(\frac{\varphi}{\lambda}\right)^2\right\}. \tag{34}$$

This elastic–plastic state terminates when plastic hinges again form at the ends of the brace, and a mechanism results when, for a given value of λ, δ and φ satisfy eqns (30) and (34).

Since the values of $\bar{\lambda}$ and λ^* are very close as shown in eqn (20) and Table 1, the value of p is nearly equal to unity when the plastic hinges at the ends start to unload at $\varphi = \pi$, and thus the value of $\bar{\xi}$ given by eqn (26) is nearly equal to zero. The numerical calculation is therefore very sensitive to φ and $\bar{\xi}$ for this range of λ, i.e. $\bar{\lambda} < \lambda < \lambda^*$.

Case 2: $\lambda \geq \lambda^*$. For $\lambda \geq \lambda^*$, interior plastic hinges form at $\xi = \xi^*$ and $\xi = 1-\xi^*$ at the termination of the elastic state. As in Case 1(b), the plastic hinges divide the brace into three domains with the same boundary and continuity conditions except that, in this case, the slope at the ends vanishes, i.e. $\alpha = 0$. Therefore eqns (29a–c) to eqn (34) inclusive are applicable to this case with $\alpha = 0$ and $\bar{\xi}$ replaced by ξ^*.

Case 2(a): $\lambda^* \leq \lambda < \hat{\lambda}$. Referring to eqn (8), observe that $m(0)$ is positive if $0 < \varphi < 2\pi$. In view of eqns (7) and (14), if $\varphi < 2\pi$ when the elastic state terminates as defined by loading Stage 2 in Fig. 4(c), the brace can sustain further load in the elastic–plastic state as shown in Fig. 4(a) as the stress points move from loading Stages 2 to 3. Observe that the maximum moment occurs at $\xi = \xi^* = 0.169$ at loading Stage 2 and remains there through subsequent loading stages. Furthermore it decreases from loading Stages 2 to 3, and increases again after loading Stage 3, the incipient mechanism state.

Case 2(b): $\lambda \geq \hat{\lambda}$. If $\phi > 2\pi$ when the elastic state terminates as defined by loading Stage 2 in Fig. 5(c), the $h-\delta$ curve unloads from points 2 to 3 in the elastic–plastic state as shown in Fig. 5(a) as the stress points move from loading Stages 2 to 3.

The value of $\hat{\lambda}$ is determined by eliminating δ from two equations relating δ to λ, which are obtained by setting $\phi - 2\pi$ in eqns (7) and (14). For $\mu = 1.05$, the values of $\hat{\lambda}$ are tabulated in Table 1 for typical values of ϵ_y and θ.

In the above analysis, it is tacitly assumed that the interior plastic hinges which form at $\xi = \xi^*$ and $\xi = 1-\xi^*$ at the initiation of the elastic–plastic state remain stationary. This assumption is verified by numerical calculations.

Mechanism state

Case 1(a): $0 < \lambda \leq \bar{\lambda}$. As discussed before, in this range of λ, the mechanism state is reached when $p = 1$ and the value of δ at incipient plastic collapse, indicated by loading state 4 in Fig. 3(a), is given by

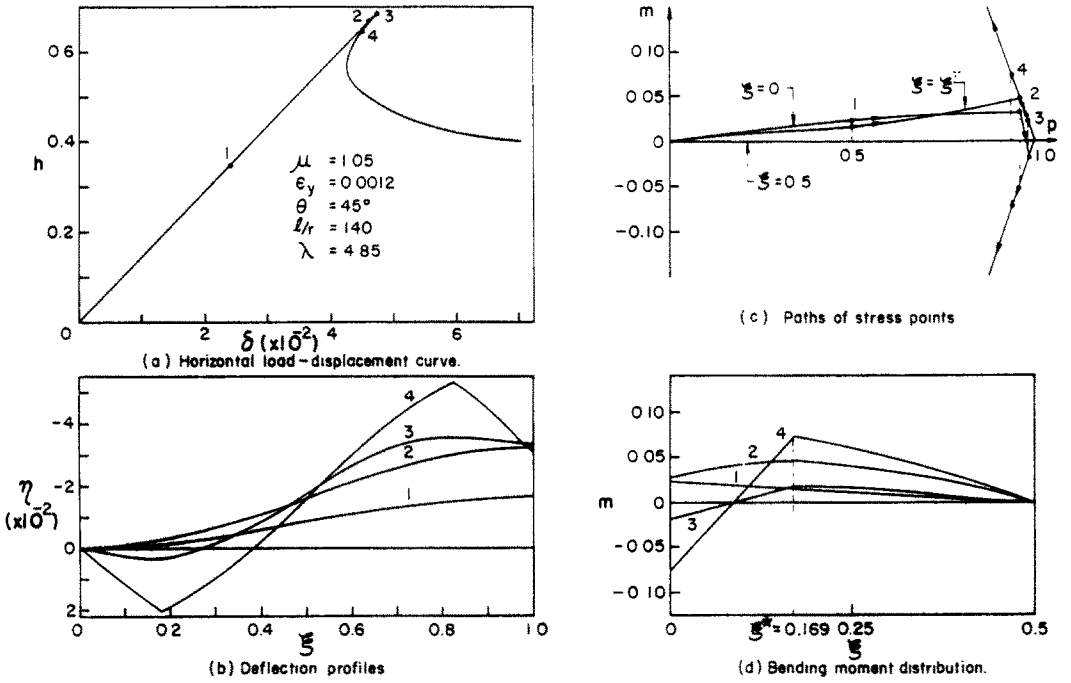

Fig. 4. Behavior of a medium brace, Case 2(a).

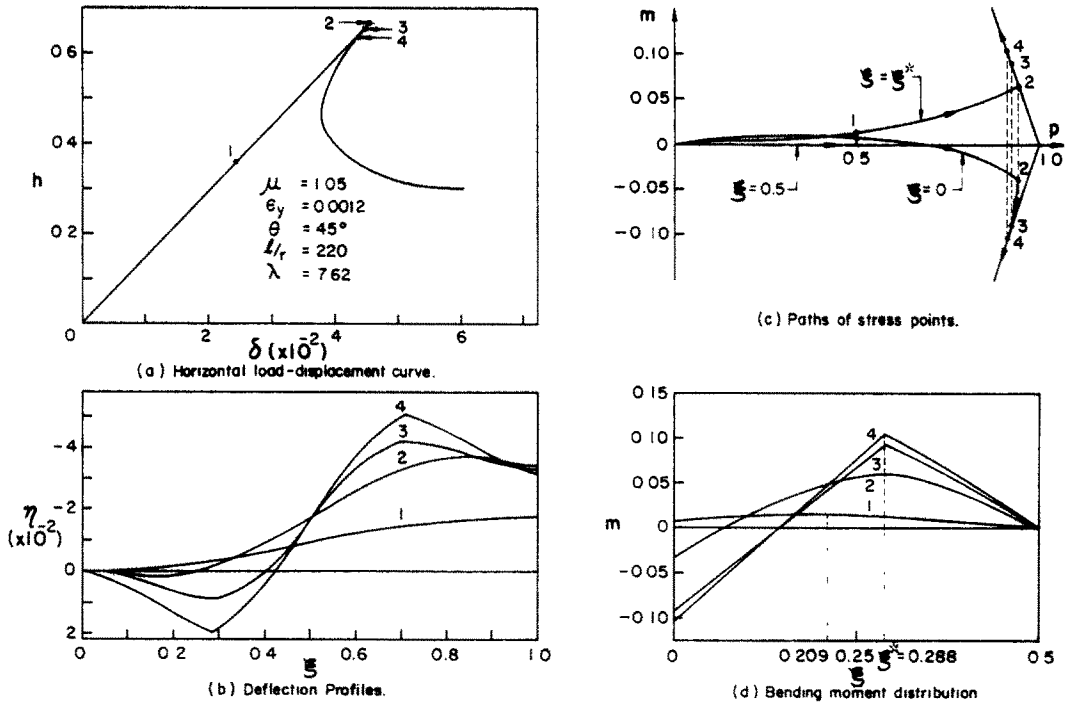

Fig. 5. Behavior of medium brace, Case 2(b).

$$\delta = \frac{\cos\theta - \sqrt{(\cos^2\theta - 2\epsilon_y \sin^2\theta)}}{\sqrt{\epsilon_y}\sin^2\theta} \tag{35}$$

obtained from the solution of eqn (17) with ϕ/λ set equal to unity. It is of interest to note that the brace assumes a straight configuration at loading Stage 4 in Fig. 3(b).

Case 1(b): $\bar{\lambda} < \lambda < \lambda^*$. In this range of λ, when δ and ϕ satisfy eqns (30) and (34) at the termination of the elastic–plastic state, the second pair of plastic hinges form at the ends. In this

case, the brace is divided into three domains and the solutions $\eta_1(\xi)$ for $0 \leq \xi \leq \bar{\xi}$ and $\eta_2(\xi)$ for $\bar{\xi} \leq \xi \leq 1/2$ must be considered. The boundary and continuity conditions defined by eqns (28a–c) remain valid with the exception that the second condition in eqn (28a) becomes

$$\text{at} \quad \xi = 0, \quad m_1(0) = -1.18(1-p). \tag{36}$$

Following similar procedure as before leads to

$$\eta_1(\xi) = \frac{1.18\lambda}{\mu\varphi^2 \sin\varphi\bar{\xi}}\left\{1-\left(\frac{\varphi}{\lambda}\right)^2\right\}\{\sin\varphi(\xi-\bar{\xi}) + \sin\varphi\xi + (1-2\xi)\sin\varphi\bar{\xi}\} - \delta\xi\sin\theta \quad \text{for} \quad 0 \leq \xi \leq \bar{\xi} \tag{37a}$$

$$\eta_2(\xi) = \frac{1.18\lambda}{\mu\varphi^2 \sin\varphi(1/2-\bar{\xi})}\left\{1-\left(\frac{\varphi}{\lambda}\right)^2\right\}\left\{\sin\varphi\left(\frac{1}{2}-\xi\right) + (1-2\xi)\sin\varphi\left(\frac{1}{2}-\bar{\xi}\right)\right\}$$

$$-\delta\xi\sin\theta \quad \text{for} \quad \bar{\xi} \leq \xi \leq \frac{1}{2}. \tag{37b}$$

Substituting eqns (37a,b) in eqn (6) yields an axial force-displacement relation similar in form as eqn (30) but, in this case, the functions B_2, B_3 and B_4 defined in eqn (31a–c) take the form

$$B_2 = -\delta\sin\theta - \frac{2.36\lambda}{\mu\varphi^2}\left\{1-\left(\frac{\varphi}{\lambda}\right)^2\right\} \tag{38a}$$

$$B_3 = \left(\frac{1.18\lambda}{\mu\varphi^2}\right)\left\{1-\left(\frac{\varphi}{\lambda}\right)^2\right\}\frac{1+\cos\varphi\bar{\xi}}{\sin\varphi\bar{\xi}} \tag{38b}$$

$$B_4 = -\frac{1.18\lambda}{\mu\varphi^2}\left\{1-\left(\frac{\varphi}{\lambda}\right)^2\right\}. \tag{38c}$$

The expressions for the bending moments and the horizontal force become respectively,

$$m_1(\xi) = 1.18\left\{1-\left(\frac{\varphi}{\lambda}\right)^2\right\}\frac{\sin\varphi(\xi-\bar{\xi}) + \sin\varphi\xi}{\sin\varphi\bar{\xi}} \tag{39a}$$

$$m_2(\xi) = 1.18\left\{1-\left(\frac{\varphi}{\lambda}\right)^2\right\}\frac{\sin\varphi(1/2-\xi)}{\sin\varphi(1/2-\bar{\xi})} \tag{39b}$$

$$h = \left(\frac{\varphi}{\lambda}\right)^2\left[\cos\theta + 2.36\sin\theta\left(\frac{\lambda\sqrt{\epsilon_y}}{\mu\varphi^2}\right)\left\{1-\left(\frac{\varphi}{\lambda}\right)^2\right\} + \delta\sqrt{\epsilon_y}\sin^2\theta\right] \tag{40}$$

Case 2: $\lambda \geq \lambda^*$. In this case, when δ and φ satisfy eqns (30) and (34) with $\alpha = 0$ and $\bar{\xi}$ replaced by ξ^* at the termination of the elastic–plastic state, the second pair of plastic hinges form at the ends as in Case 1(b) and the solutions, eqns (37a,b)–(40) inclusive, are applicable with $\bar{\xi}$ replaced by ξ^*.

It is of interest to note that the mechanism states of Case 2(a) and Case 2(b) are governed by the same set of equation discussed above. The absolute values of the moment at $\xi = 0$ and $\xi = \xi^*$ are equal throughout this state starting from incipient mechanism state, loading Stage 3 in Figs. 4(d) and 5(d), in which a typical mechanism state is indicated by loading Stage 4.

For long braces, the unloading horizontal load-displacement curves in the elastic–plastic and mechanism states are unstable. The maximum load for such a brace occurs at the termination of the elastic state and agrees well with the elastic buckling load of a fixed end column buckling in an anti-symmetrical mode. This load corresponds to the smallest root of the equation obtained by setting the denominator of eqn (8), the expression for the bending moment in elastic state, equal to zero.

3. EXPERIMENTAL INVESTIGATION

Test specimens

The typical test specimen shown in Fig. 6(a) is designed to simulate a braced frame system such as the one shown in Fig. 6(d) in such a way that only the lateral load resisted by the diagonal braces is measured in the tests. The specimen is made up of two braces of box section, 50 mm square and 2 mm thick, welded at the top to a heavy wide-flange loading block. The mechanical properties of the material shown in Table 2 are average values obtained from tension tests performed in accordance with ASTM Standards A370-68[12].

Test setup

Figure 7 shows a schematic diagram of the test apparatus, and an overall view of a typical test setup is shown in Fig. 8. In order to prevent the rotation and lateral translation of the loading block, sixteen steel stay rods of 0.5 in. diameter, attached to the loading block, are installed with approximately 300 kg of pretension force in each rod prior to the test. The downward movement of the loading block, i.e. Δ shown in Figs. 1 and 6(d), is measured by the dial gage G in Fig. 7. The transverse deflection of each brace are measured by a group of dial gages H placed at equal intervals along the length of the brace. The rotation and lateral translation of the loading block, if any, are detected by five dial gages J in Fig. 7(c). The initial crookedness of the braces after welding to the base beam, measured in terms of transverse deviation from line *ab* in Fig. 6(a), was found to be less than 0.24% of the length of the brace in all test specimens. The effects of initial crookedness and residual stresses are not considered in this study.

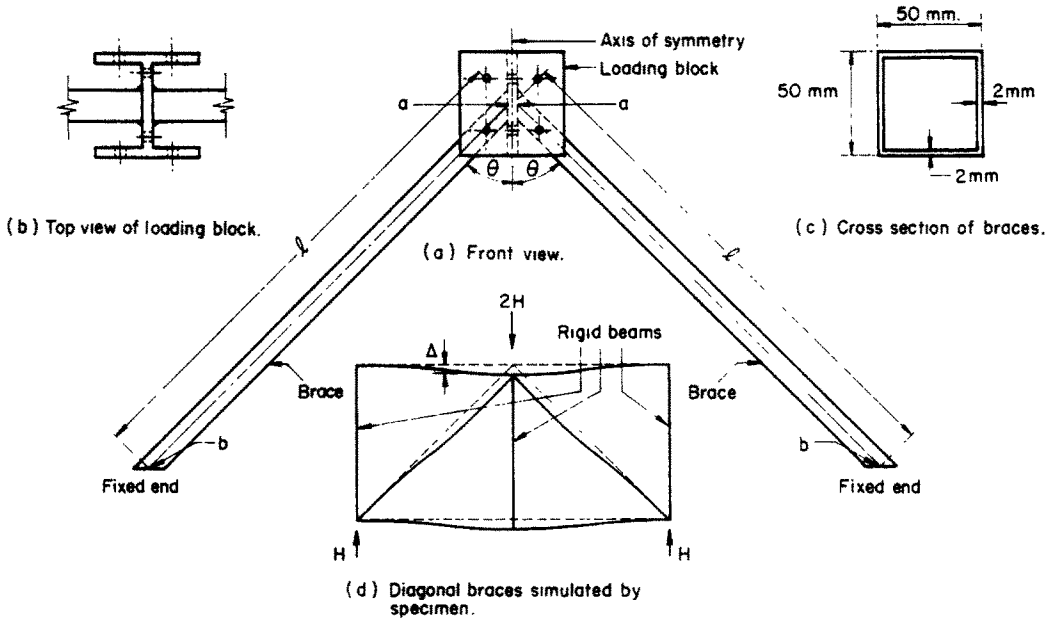

Fig. 6. A typical test specimen with loading block.

Table 2. Dimensions and properties of test specimens

Specimen No.	Case	ℓ(cm)	I(cm^4)	A(cm^2)	Z_p(cm^3)	ℓ/r	λ	θ(degree)
1	1	100.0	17.47	4.219	7.876	49.1	1.90	45
2	2	210.0	17.47	4.218	7.877	103.2	3.99	30
3	2	198.0	17.47	4.220	7.878	97.3	3.76	45
4	2	205.0	17.47	4.219	7.877	100.7	3.89	60
5	2	295.0	17.47	4.220	7.876	144.9	5.60	45

Mechanical properties:

σ_y = 3,076 kg/cm^2, E = 2,059 x 10^3 kg/cm^2, ε_y = 0.001494

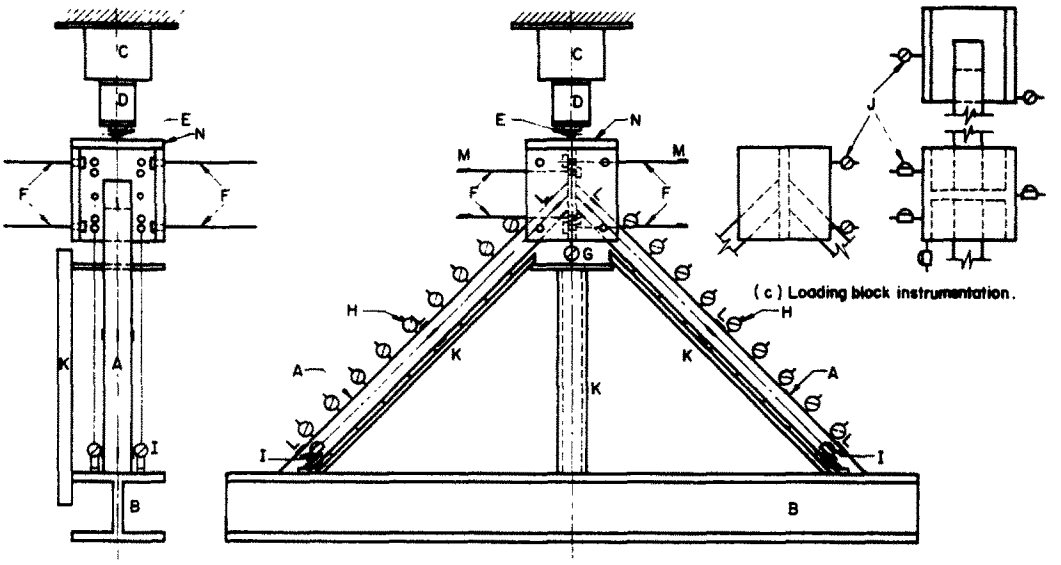

A Test specimen B Base beam C Hydraulic jack D Load cell E Ball bearing
F Stay rods G Dial gage H Dial gages I Dial gages J Dial gages
K Dial gage support stand L Strain gages M Strain gages N Loading block

Fig. 7. Test setup.

Fig. 8. A typical test setup.

The axial strains in each brace are measured by three sets of four wire strain gages L, each set mounted along the middle lines of the four faces of the box section. The axial strains in the stay rods at each stage of loading are measured by wire strain gages M. When the loading block moves downward under applied load, the tensions in the stay rods are recorded and their components in the vertical direction are subtracted from the reading of the load cell (D) to yield the load carried by the braces.

Test results

The test results obtained for the five specimens listed in Table 2 are shown in Figs. 9–13 in the form of horizontal load-displacement curves and deflection profiles. The theoretical results predicted by the proposed analysis are also plotted in the figures for comparison. The latter are based on a piecewise linear approximation to the actual interaction curve for box section determined for the specimens tested, as shown in Fig. 2. Observe that the actual and approximate curves are practically identical in the range $0.45 \leq p \leq 1$, which is the range of interest. The values of μ computed for all five specimens are equal for practical purposes and taken equal to 1.0899.

The experimental and theoretical $h - \delta$ curves agree very well in the elastic range. Test specimen No. 1 falls under Case 1(a) in which $\lambda < \bar{\lambda}$. The theoretical prediction that the braces attain the maximum load at incipient plastic collapse was clearly observed experimentally as shown in Fig. 11(a). Gradual unloading takes place after the displacement increases and out-of-plane buckling occurs at large displacement at which rotation and lateral translation of the loading block were observed. The deflection profiles shown in Fig. 9(b) agree well and both the experimental and theoretical profiles are straight in the plastic collapse state as predicted.

The other four specimens belong to Case 2 in which $\lambda > \lambda^*$. Figures 9(a)–13(a) show that both theoretical maximum load and the stable segment of the unloading branch of the $h - \delta$ curve with positive slope which follows were not observed experimentally. Due to initial crookedness, residual stresses and imperfect symmetry of the specimens, δ increases rapidly in the experimental curve which differs from the stable elastic branch of the theoretical curve and

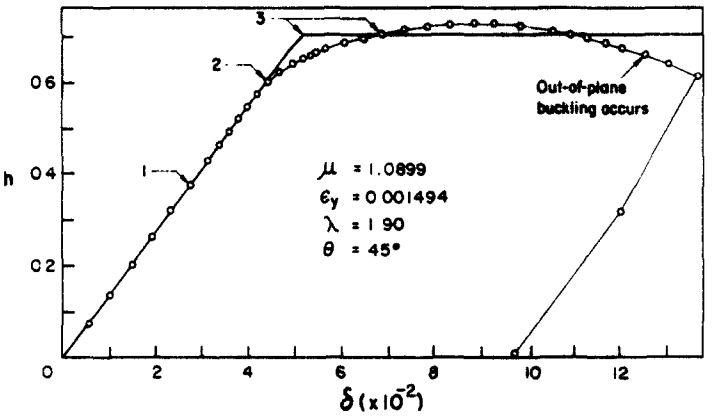

(a) Horizontal load-displacement curves

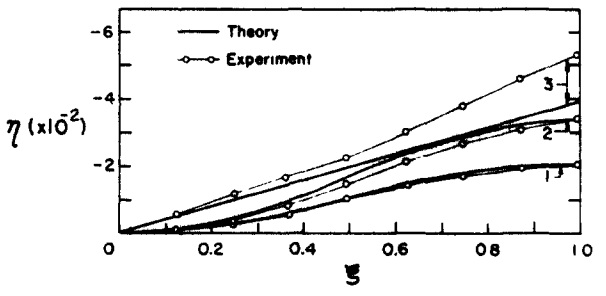

(b) Deflection profiles.

Fig. 9. Test specimen No. 1, Case 1.

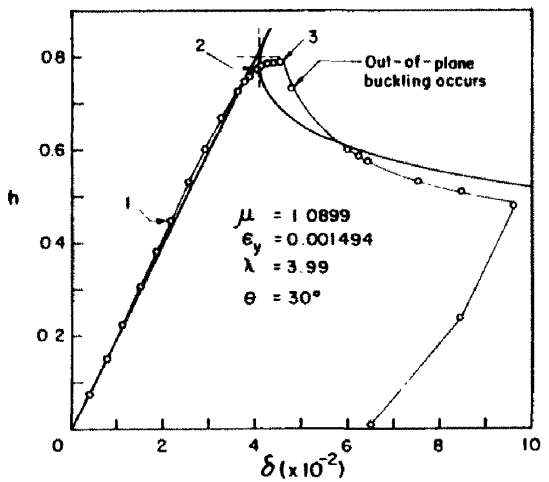

(a) Horizontal load-displacement curves

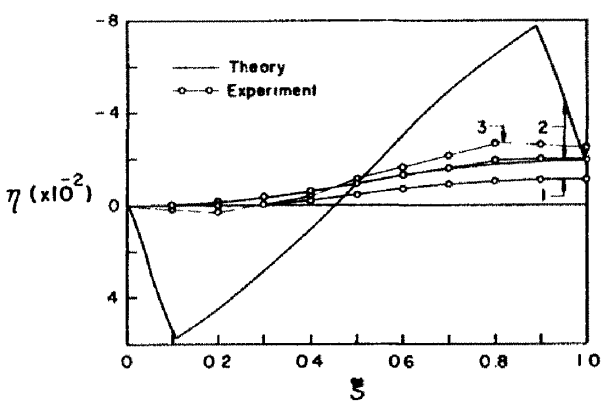

(b) Deflection profiles.

Fig. 10. Test specimen No. 2, Case 2.

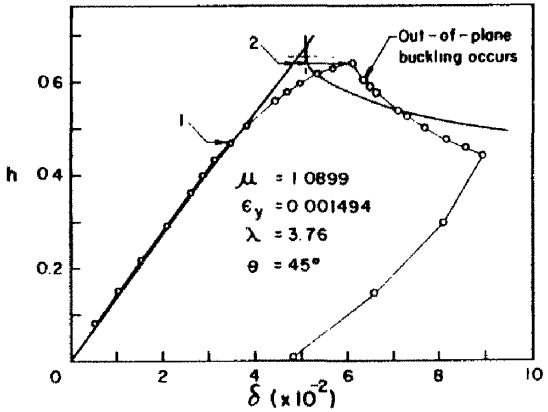

(a) Horizontal load-displacement curves

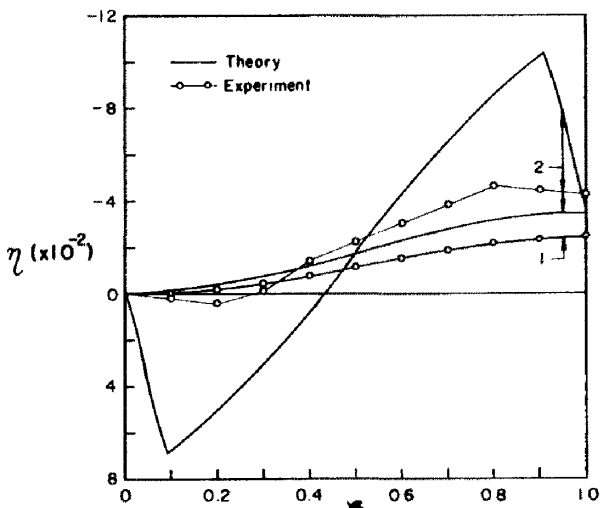

(b) Deflection profiles.

Fig. 11. Test specimen No. 3, Case 2.

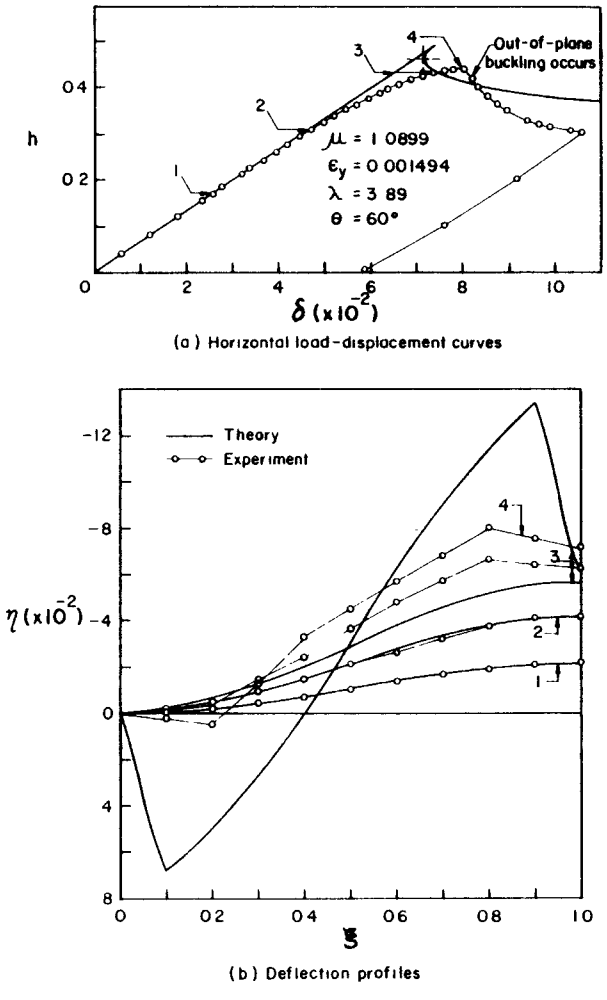

Fig. 12. Test specimen No. 4, Case 2.

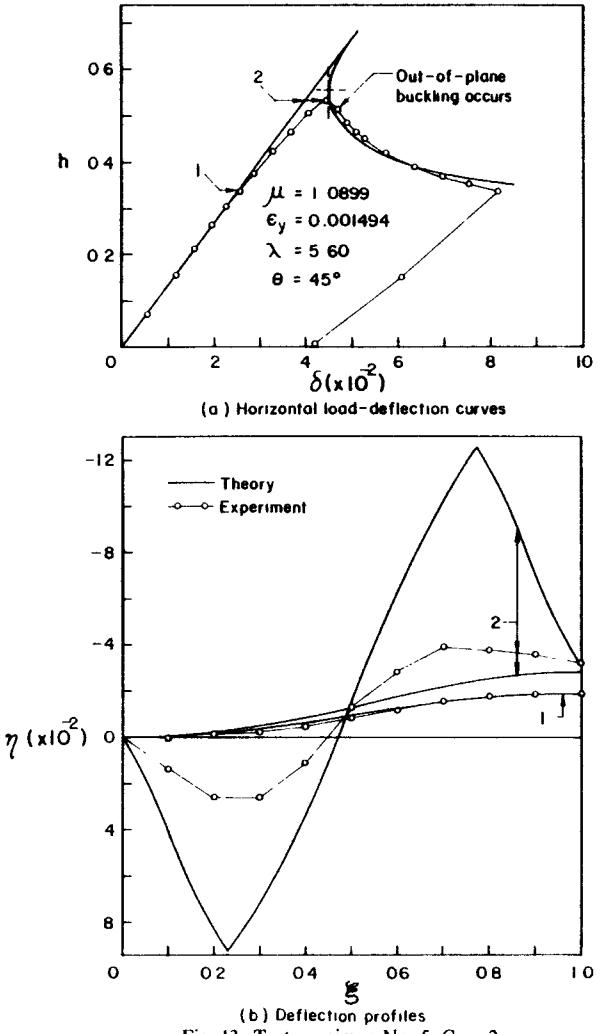

Fig. 13. Test specimen No. 5, Case 2.

approaches the unstable branch in the vicinity of the point on the unloading curve where the slope is vertical. It is obvious that the effect of initial imperfections, such as crookedness and residual stresses, is responsible for the difference between the theoretical and the experimental results. However, it is important to observe that the experimental maximum loads of braces with unavoidable initial imperfections consistently approximate the theoretical loads predicted by this point.

The deflection profiles shown in Figs. 9(b)–13(b) demonstrates excellent agreement in the elastic range. Although the experimental curve deviates from the theoretical one in the vicinity where the slope of the theoretical curve becomes vertical, the shape of two profiles nevertheless remains similar and deviates only in amplitude. Out-of-plane buckling occurs soon after the experimental maximum loads are reached when rotation and lateral translation of the loading block take place. In the theoretical analysis, it is tacitly assumed that the interior plastic hinge locations remain stationary. The kinks in both the theoretical and experimental deflection profiles bear out this assumption.

In all the four tests, out-of-plane buckling occurs after the maximum load is reached because of the torsionally weak support condition at the top of the specimen. Thus, the experimental unloading curves after out-of-plane buckling takes place cannot be compared with the theoretical curve. However, it is believed that this support condition did not affect the in-plane behavior of the brace before out-of-plane buckling occurs, since no significant rotation and lateral translation were observed by the monitoring dial gages on the loading block until after the maximum load carrying capacity of the braces is reached.

4. DISCUSSION AND CONCLUSION

Post-buckling behavior of short-columns

It is interesting to compare the results of the proposed analysis with those given by Paris[1] and Nonaka[8], both of whom dealt with a simply supported bar subjected to a compressive axial load. The axial load-displacement relation is linear in the elastic range. They assumed that, for the short bar, lateral deflection must occur when the load reaches the yield load and a plastic hinge develops at the mid-point of the bar whose behavior is governed by an assumed yield condition. The post-yielding axial load-displacement curve unloads in the mechanism state and is unstable. In Fig. 9(a), the theoretical curve shows that specimen No. 1, a short brace, sustains the maximum load after axial yielding occurs at incipient plastic collapse. This prediction is confirmed by the experimental curve in the same figure, and the same phenomena were observed in the experimental investigation by Paris[1].

Parametric study

An investigation on compact wide-flange column sections with depth from 4 to 14 in. reveals that μ ranges from 1.04 to 1.06 with a mean value of 1.05. Lee and Hauck[13] found that the values of R, the ratio of the flange area to be web area, for a similar grouping of wide-flange column sections with depth from 8 to 14 in., range from 2.9 to 3.6 and suggested that $R = 3.25$, which is a median and a mean value, be used in general study since the column strength is relatively insensitive to minor variation in R. The value of μ corresponding to $R = 3.25$ is 1.041. On the other hand, μ can also be expressed by $d/(2fr)$ where d and f denote the depth and the shape factor of the wide-flange section, respectively. Galambos[14] observed that the value of d/r is nearly constant and approximately equal to 2.38. The value of f for wide-flange column sections ranges from 1.10 to 1.23 with an average of 1.137 and a mode of 1.115[15]. The values of μ corresponding to $d/r = 2.38$ and $f = 1.137$ and 1.115 are 1.047 and 1.067, respectively. In the following parametric study of horizontal load-displacement relations, μ will be taken equal to 1.05 and the other parameters considered are: $\theta = 30°, 45°, 60°$; $\lambda = 2.08$ to 13.86 ($l/r = 60$ to 400) and $\epsilon_y = 0.0012$.

Horizontal load-displacement relation. Figures 14(a–c) show the behavior of h plotted vs arguments of δ for various values of λ with $\mu = 1.05$, $\epsilon_y = 0.0012$ and $\theta = 30°$, 45° and 60°. Observe from these curves that the point with vertical slope will appear only in the middle range of λ. The same phenomenon is observed in the numerical results obtained by Paris[1] for a simply supported column whose yield load and Euler load are nearly equal.

Horizontal load-slenderness ratio relation. Figure 15 shows, in solid lines, the variation of

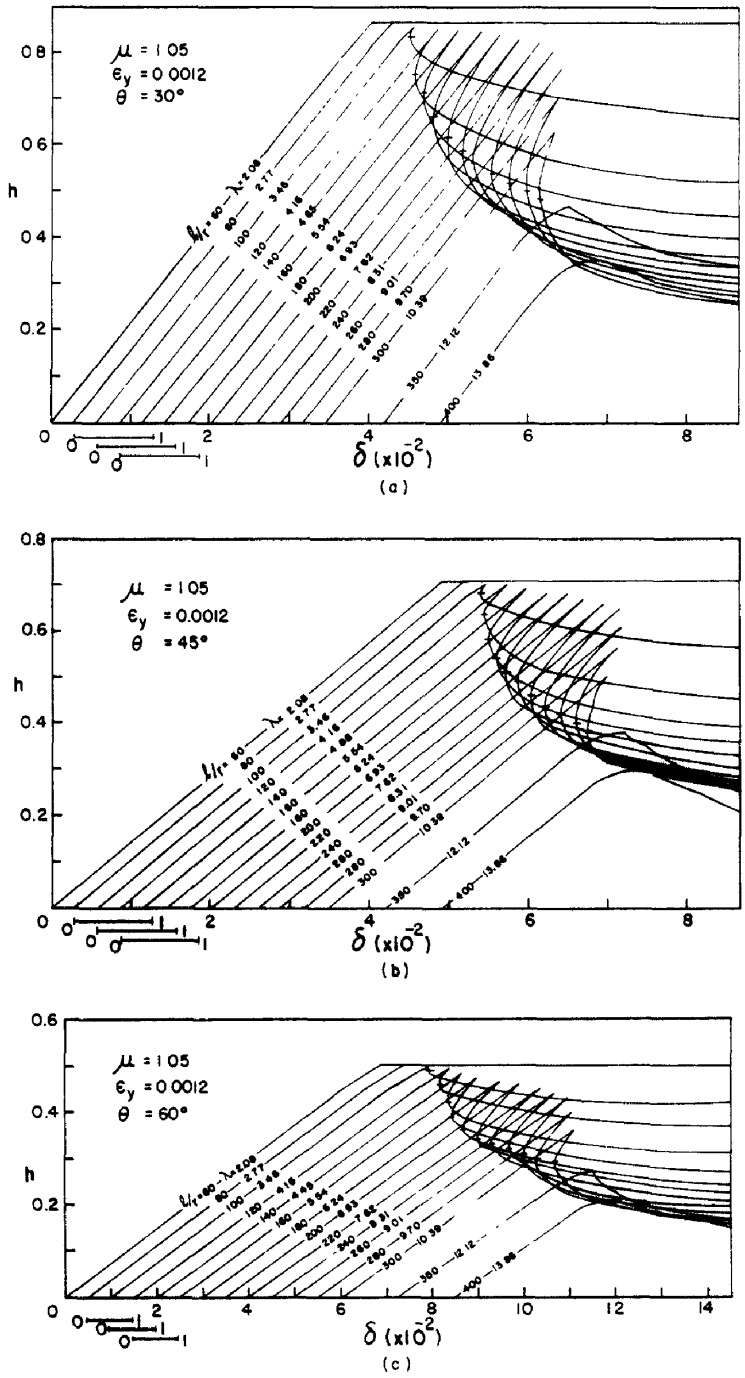

Fig. 14. Horizontal load-displacement curves.

the horizontal load h^* plotted vs arguments of the slenderness ratio λ for the various values of θ, where h^* denotes the smaller of either the maximum load or the load at which the slope of the horizontal load–displacement curve becomes infinity. The dashed lines show the values of $p^* \cos\theta$ where p^* is the axial force corresponding to h^*. The two sets of curves are almost identical since the contribution of the shear force to h^* is very small in comparison with that of $p^* \cos\theta$.

Conclusion

Figure 16 shows, in solid lines, the variation of the axial force p^* plotted vs arguments of λ for various values of θ. The dotted lines represent the maximum axial force and the dashed lines the tangent modulus load and the elastic buckling load p_c of a fixed-end column buckling in

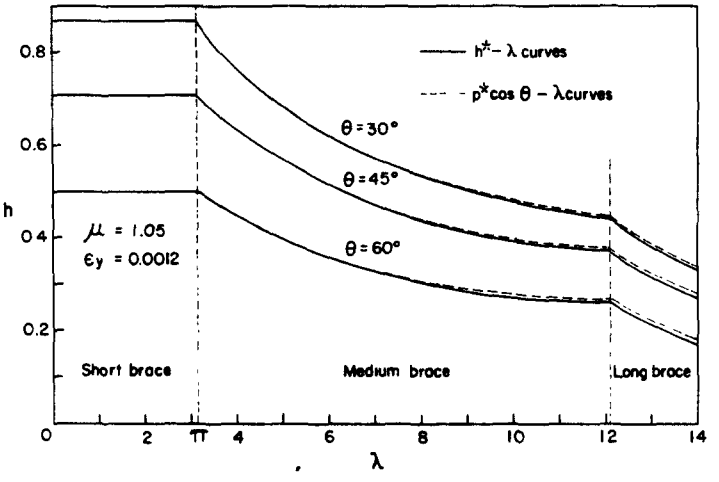

Fig. 15. Horizontal load-slenderness ratio curves.

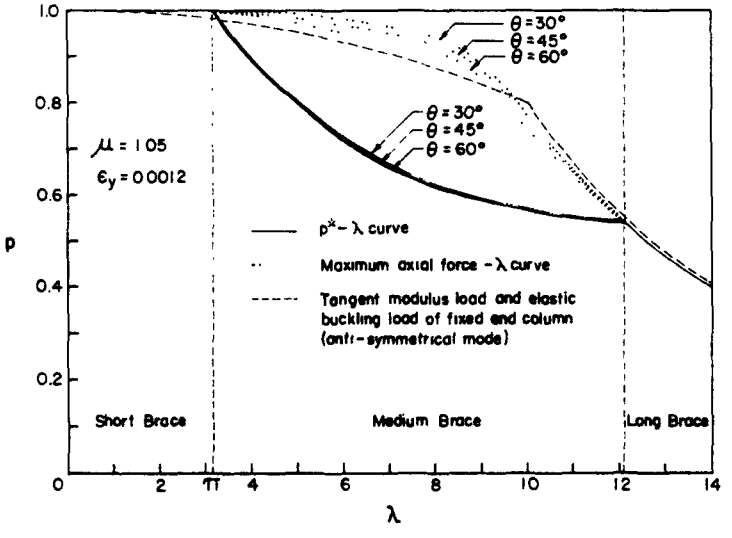

Fig. 16. Axial load-slenderness ratio curves.

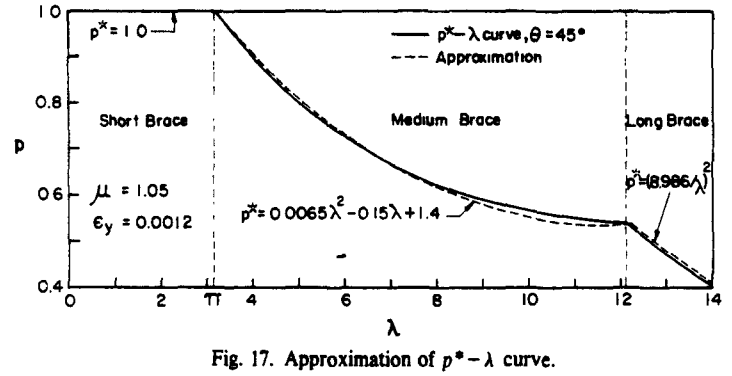

Fig. 17. Approximation of $p^* - \lambda$ curve.

anti-symmetrical mode. The latter is given by

$$p_c = (8.986/\lambda)^2. \tag{41}$$

Observe in eqn (8) that $m(\xi)$ approaches infinity as ϕ approaches 8.986. The tangent modulus load is obtained assuming that the tangent modulus ratio $\tau = E_t/E$ is given by [16]

$$\tau = \frac{(\sigma_y - \sigma_c)\sigma_c}{(\sigma_y - \sigma_p)\sigma_p} \tag{42}$$

in which E_t, σ_c and σ_p denote the tangent modulus, the critical stress and the proportional limit, respectively. In this analysis, σ_p is taken equal to $0.8\sigma_y$.

It is interesting to note that the maximum axial force agrees well with the tangent modulus load and the elastic buckling load. The effect of θ on $p^* - \lambda$ curves in the range studied, $30° \leq \theta \leq 60°$, is small and can be neglected. In Fig. 17, the $p^* - \lambda$ curve for $\theta = 45°$ is shown in solid line with the results of the following empirical formulas in dashed line:

$$p^* = 1 \quad \text{for} \quad 0 < \lambda \leq \pi \tag{43a}$$

$$p^* = 0.0065\lambda^2 - 0.15\lambda + 1.4 \quad \text{for} \quad \pi \leq \lambda \leq 12.2 \tag{43b}$$

$$p^* = (8.986/\lambda)^2 \quad \text{for} \quad 12.2 \leq \lambda. \tag{43c}$$

Since the value of the horizontal load h^* is very close to $p^* \cos\theta$, for practical purposes, it can be simply obtained by $h^* = p^* \cos\theta$, where the value of p^* is given in eqns (43a–c).

REFERENCES

1. P. C. Paris, Limit design of columns. *J. Aeronaut. Sci.* 21(1), 43–49 (1954).
2. N. W. Murray, The determination of the collapse loads of rigidly jointed frameworks with members in which axial forces are large. *Proc. ICE, Part* 3, Vol. 5, 213–232 (April 1956).
3. N. W. Murray, Further tests on braced frameworks. *Proc. ICE*, Vol. 10, 503–516 (August 1958).
4. J. G. Nutt, The collapse of triangulated trusses by buckling within the plane of the truss. *Structural Engr* 37(5), 141–149 (1959).
5. B. G. Neal and D. M. Griffith, The collapse of rigidly-jointed singly redundant light alloy trusses. *Structural Engr* 41(12), 399–405 (1963).
6. M. Wakabayashi, C. Matsui, K. Minami and I. Mitani, Inelastic behavior of steel frames subjected to constant vertical and alternating horizontal loads. *Proc. 5th World Conf. Earthquake Engng*, No. 146, 1194–1198, Rome (June 1973).
7. S. Igarashi, K. Inoue, M. Kibayashi and M. Asano, Hysteretic characteristics of steel braced frames. *Trans. Arch. Inst. Japan, No.* 196, 47–54 (June 1972) (in Japanese).
8. T. Nonaka, An elastic–plastic analysis of a bar under repeated axial loading. *Int. J. Solids Structures* 9(5), 569–580 (1973).
9. A. B. Higginbotham, The Inelastic Cyclic Behavior of Axially Loaded Steel Member, Ph.D. Dissertation, 15–24. University of Michigan, Ann Arbor (Jan. 1973).
10. M. Shibata, T. Nakamura, N. Yoshida, S. Morino, T. Nonaka and M. Wakabayashi, Elastic–plastic behavior of steel braces under repeated axial loading. *Proc. 5th World Conf. Earthquake Engng*, Rome, No. 100, 845–849 (June 1974).
11. A. Wada, F. Suto and M. Fujimoto, Non-linear analysis for *K*-type braced steel frames. *Prelim. Rep., Symp. Resistance and Ultimate Deformability of Structures Acted on by Well Defined Repeated Loads, IABSE*, Lisbon, 29–34 (Sept. 1973).
12. Standard Methods and Definitions for Mechanical Testing of Steel Products, *ASTM Standard* A370–68, 359–372 (1970).
13. S. L. Lee and G. F. Hauck, Buckling of steel columns under arbitrary end loads. *J. Struct. Div., ASCE* 90(ST2), 179–200 (1964).
14. T. V. Galambos, *Structural Members and Frames*, pp. 96–98. Prentice Hall, New Jersey (1968).
15. Plastic Design in Steel—A Guide and Commentary, *ASCE Manual* 41, 2nd Edn, pp. 36–40 and 128–137 (1971).
16. F. Bleich, *Buckling Strength of Metal Structures*, pp. 51–54. McGraw-Hill, New York (1952).